Earth and Planetary Science Letters 409 (2015) 157–167

Contents lists available at ScienceDirect

Earth and Planetary Science Letters

www.elsevier.com/locate/epsl

New bulk sulfur measurements of Martian meteorites and modeling the fate of sulfur during melting and crystallization – Implications for sulfur transfer from Martian mantle to crust–atmosphere system

Shuo Ding [a,*], Rajdeep Dasgupta [a], Cin-Ty A. Lee [a], Meenakshi Wadhwa [b]

[a] Department of Earth Science, Rice University, 6100 Main street, MS 126, Houston, TX 77005, USA
[b] School of Earth and Space Exploration, Arizona State University, AZ, USA

ARTICLE INFO

Article history:
Received 26 June 2014
Received in revised form 23 October 2014
Accepted 27 October 2014
Available online xxxx
Editor: B. Marty

Keywords:
Mars
deep sulfur cycle
Martian meteorites
mantle melting
fractional crystallization
crust formation

ABSTRACT

Sulfur storage and transport between different reservoirs such as core, mantle, crust and atmosphere of Mars are tied to igneous processes. Martian meteorites carry a record of mantle melting and subsequent differentiation history of Martian magmas. Investigation of S geochemistry of Martian meteorites can thus provide an understanding of how S is transferred from the Martian interior to the exosphere. In this study we measured bulk S concentration of 7 Martian meteorites and modeled the behavior of S during both isobaric crystallization of primary Martian magmas and isentropic partial melting of Martian mantle. Comparisons between measured data and modeled results suggest that (1) sulfides may become exhausted at the source during decompression melting of the mantle and mantle-derived basalts may only become sulfide-saturated after cooling and crystallization at shallow depths and (2) in addition to degassing induced S loss, mixing between these differentiated sulfide-saturated basaltic melts and cumulus minerals with/without cumulate sulfides could also be responsible for the bulk sulfur contents in some Martian meteorites. In this case, a significant quantity of S could remain in Martian crust as cumulate sulfides or in trapped interstitial liquid varying from 2 to 95 percent by weight. Our modeling also suggests that generation of sulfide-undersaturated parental magmas requires that the mantle source of Martian meteorites contain <700–1000 ppm S if melting degree estimation of 2–17 wt.% based on compositions of shergottites is relevant.

1. Introduction

Sulfur fluxes and storage are important in understanding processes of terrestrial planets from the core to exosphere. Sulfur is thought to be a dominant volatile element on Mars (Gaillard et al., 2012; Gibson et al., 1985; King and McLennan, 2010; Stewart et al., 2007). Understanding S distribution among Martian mantle, crust and the atmosphere as well as the fate of sulfur in various magmatic processes is important for constraining the differentiation history of Mars.

The primary source of sulfur to the Martian surface–atmosphere system is volcanism (Gaillard and Scaillet, 2009; Halevy et al., 2007; Johnson et al., 2008). Further the distribution of S between Martian crust and atmosphere, which can potentially affect the ancient climate on Mars and the formation of sulfate deposits on the surface, is also intimately related to the behavior of sulfur during magmatic differentiation including cooling, crystallization, and degassing. The amount of S released to the Martian atmosphere may be estimated as the difference between (1) the S content of the mantle-derived magma and (2) the budget of magmatic S trapped in the basaltic crust. The former could be estimated by S contents of basaltic melts at sulfide saturation (SCSS) (Ding et al., 2014; Righter et al., 2009), assuming mantle derived magma is sulfide saturated. The latter is usually approximated by S contents in Martian meteorites, although bulk S concentration data of the latter remained limited until recently (Franz et al., 2014; Lodders, 1998). Based on the assumptions that erupted Martian basalts are sulfide saturated and the difference between the expected solubility limit and the measured concentration in olivine-phyric shergottites reflects S loss owing to degassing, Righter et al. (2009) estimated that mantle derived basalts on Mars degassed 2400 ppm S. Similar approaches are also applied to constrain sulfur degassing flux for terrestrial settings (e.g., Self et al., 2008; Zhang et al., 2013). However, both above assumptions can be problematic. First, it is not considered whether sulfide, if present in the Martian mantle, can remain in the residue during partial melting;

* Corresponding author.
E-mail address: sd35@rice.edu (S. Ding).

http://dx.doi.org/10.1016/j.epsl.2014.10.046
0012-821X/

Second, most Martian meteorites contain cumulus minerals and some have experienced secondary alteration (weathering/impact effects), which could either deplete or enrich S in meteorites. Another approach to estimate magmatic degassing of S is by simulating equilibrium degassing of primary magmas, which has been quantitatively investigated by Gaillard et al. (2012). A maximum of 2100 ppm S degassing from an initial concentration of 3500 ppm S in primitive Martian magmas is obtained in Gaillard et al. (2012) for hydrated-oxidized melts (0.4 wt.% H_2O, FMQ-0.5). The calculations by Gaillard et al. (2012) consider several parameters, such as atmospheric pressure, oxygen fugacity of emplaced magmas and other volatiles (H_2O and CO_2) contents in the melts, for the degassing process. However, these authors do not consider the possible SCSS and S concentration changes in the evolving melt before degassing, though by analogy to the case on Earth, both SCSS and S concentration in the melt must change during fractional crystallization because SCSS is a function of pressure, temperature, oxygen fugacity, and melt composition (Baker and Moretti, 2011; Holzheid and Grove, 2002; Jégo and Dasgupta, 2013, 2014; Jugo, 2009; Jugo et al., 2010; Lee et al., 2012; Li and Ripley, 2009; Liu et al., 2007) which in turn would control the onset of sulfide precipitation. How sulfur behaves during emplacement and crystallization of basalt into the crust is a missing link in sulfur cycle. Magmatic S budget of Martian crust is key information in this regard, which needs to be evaluated in the context of differentiation of primitive Martian basalts. Therefore here we focus on S budgets of Martian meteorites.

Martian meteorites range from evolved basaltic shergottites with small fractions of phenocrysts to cumulates with small or negligible amount of trapped liquids. Sulfur contents of different types of Martian meteorites thus can provide important insights into igneous processes that operated on Mars. Righter et al. (2009) calculated sulfur carrying capacity change along differentiation path of a model Martian magma taken from Symes et al. (2008) and compared the result to the S contents of some olivine-phyric and basaltic shergottites. Similarly, Ding et al. (2014) applied their new SCSS model to investigate the change in SCSS along the liquid line of descent and sulfide precipitation in corresponding cumulates derived from Yamato 98049. However, no study has combined petrology of different Martian meteorites and their bulk S data and interpreted them in the context of magma generation via melting of a sulfide-bearing mantle and differentiation of various putative parental melts via shallow fractional crystallization.

In this study we measured bulk S contents of 7 Martian meteorites using solution ICP-MS (Erdman et al., 2014) and discuss the bulk sulfur data of meteorites from this study and those from literature by modeling the fate of S during fractional crystallization of Martian magmas and the fate of sulfide during mantle partial melting. By comparing bulk S data of Martian meteorites to the modeling results, we estimate the plausible S budgets of the Martian mantle, crust, and atmosphere.

2. Methods

2.1. Analytical technique

Bulk S contents of 7 Martian meteorites (the shergottites Los Angeles, Zagami, NWA 856, NWA 1068, and Tissint, and the nakhlites NWA 998 and Nakhla) were measured using high mass-resolution solution ICP-MS following the method in Erdman et al. (2014). Interior chips of each of these Martian meteorites were obtained from the meteorite collection in the Center for Meteorite Studies at Arizona State University. Fractions, ranging from ~13 to ~60 mg, were taken from each of these interior chips. For three of the samples (NWA 856, NWA 1068 and NWA 998), two separate fractions were taken to assess sample heterogeneity. Each of these fractions was then dissolved and processed separately. One of the fractions of NWA 998 was leached with 1 mol/part HCl first. After being sonicated and centrifuged, the supernatant and solid residues were carefully separated. The supernatant was directly diluted by 1 mol/part HCl while the solid residues went through same steps as other bulk rock fractions. Sulfur in the bulk rock fractions was dissolved and converted to the S^{6+} species in the form of SO_4^{2-}. Both bulk rock solutions and the leachate were analyzed with the Thermo FinniganElement 2 magnetic sector ICP-MS at Rice University. To check the accuracy of the sulfur analyses, several terrestrial rock standards including one basalt (United States Geological Survey, BHVO-2), one gabbro (Japanese Geological Survey, JGb-1) and one marine mud (United States Geological Survey, MAG-1) were run as external standards in the same sequence. The limit of detection on sulfur ranges from 40 to 90 ppm, determined by the instrumental detection limit in solution and the dilution factor (Erdman et al., 2014).

2.2. Geochemical data compilation

We have compiled the bulk S data of Martian meteorites from this study and previous studies. 32 Martian meteorites with available bulk rock mineralogy and composition are included in Table 1. Most of the 32 Martian meteorites, including 7 measured in this study, belong to 3 groups: basaltic shergottite, ol-phyric shergottite and nakhlite. In addition, two lherzolitic shergottites (LEW88516 and ALH77005), one dunite (Chassigny) and one orthopyroxenite (ALH84001) are also included in the data compilation.

Basaltic shergottites chiefly comprise pyroxene and plagioclase without early crystallizing olivine or chromite (Papike et al., 2009). Stolper and McSween (1979) demonstrated by optical analysis and melting experiments that both Shergotty and Zagami contain cumulus pyroxene, probably without cumulus plagioclase. Cumulus pyroxenes are commonly observed in basaltic shergottites with a few exceptions such as Los Angeles (Rubin et al., 2000) and QUE94201 (McSween et al., 1996), which have been shown as liquid composition. Ol-phyric basalts share the petrographic features of olivine megacrysts, presence of chromite and Fe–Ti oxides, and low augite proportions (Goodrich, 2002; Papike et al., 2009). Textural studies and experimental results suggest that at least some olivine-phyric shergottites contain excess olivine (Filiberto and Dasgupta, 2011; Goodrich, 2003, 2002; Sarbadhikari et al., 2009; Usui et al., 2008).

Nakhlites are clinopyroxenites composed mostly of cumulus grains of subcalcic augite as the most abundant mineral and less abundant olivine and mesostasis (Treiman, 2005). Lherzolitic shergottites are also cumulates containing mainly poikilitical olivine often enclosed by pyroxene along with minor modal plagioclase (Papike et al., 2009).

Chassignites have similar texture and mineralogy to terrestrial dunites (Floran et al., 1978). Chassigny contains 91.6% olivine, 5% pyroxene, 1.7% feldspar, 1.4% chromite, 0.3% melt inclusions and trace amount of other minerals (Floran et al., 1978). Orthopyroxenite consists of only one sample, ALH84001, which contains 97% coarse grained orthopyroxene, 2% chromite, 1% plagioclase and other accessory minerals (Mittlefehldt, 1994; Papike et al., 2009).

Throughout the paper, we follow the definition of cumulus phase from Stolper and McSween (1979) as crystals accumulated or concentrated in a liquid; intercumulus liquid as the liquid from which the cumulus crystals formed and which once surrounded these crystals. Cumulate fraction refers to the mass fraction of cumulate minerals. Melt fraction refers to the mass fraction of intercumulus liquid, which is assumed to be the difference between 1 and cumulate fraction. In order to estimate the plausible fraction of cumulate minerals in Martian meteorites, we first approximate mass fraction of each mineral using the mineral modes (pyroxene,

Table 1
Bulk S concentration of Martian meteorites measured in this study and previous studies.

Name	Bulk S (ppm) and references[a]		Petrology	Possible cumulate fractions (%) and references	
This study					
Zagami	1954 ± 91	This study	basaltic shergottite	~33–45	McCoy et al. (1999); Stolper and McSween (1979)
NWA856	1584 ± 10	This study	basaltic shergottite	?	
Los Angeles	2865 ± 224	This study	basaltic shergottite	~5	Rubin et al. (2000)
NWA1068	1280 ± 48	This study	Ol-phyric shergottite	~21–26	Filiberto and Dasgupta (2011)
Tissint	2120 ± 68	This study	Ol-phyric shergottite	~8–24	Aoudjehane et al. (2012)
Nakhla	690 ± 60	This study	Nakhlite (clinopyroxenite)	~75–85	Treiman (2005)
NWA998	253 ± 42	This study	Nakhlite (clinopyroxenite)	~85	Treiman (2005)
Previous studies					
Zagami	960	Franz et al. (2014)	basaltic shergottite	~33–45	McCoy et al. (1999); Stolper and McSween (1979)
	1850	Gibson et al. (1985)			
Los Angeles	1510	Franz et al. (2014)	basaltic shergottite	~5	Rubin et al. (2000)
Shergotty	1300 ± 800	Lodders (1998)[b]	basaltic shergottite	~17	Hale et al. (1999); Stolper and McSween (1979)
	1243	Franz et al. (2014)			
EET 79001B	1930 ± 20	Lodders (1998)	basaltic shergottite	~5	McSween and Jarosewich (1983)
	576	Franz et al. (2014)			
NWA5298	465	Franz et al. (2014)	basaltic shergottite	~35	Hui et al. (2011)
Dhofar019	1630	Franz et al. (2014)	basaltic shergottite	18–22	Filiberto and Dasgupta (2011)
QUE94201	806	Franz et al. (2014)	basaltic shergottite	0	McSween et al. (1996)
DaG476	2700	Zipfel et al. (2000)	Ol-phyric shergottite	30–34	Filiberto and Dasgupta (2011)
	916	Franz et al. (2014)			
LAR06319	950	Sarbadhikari et al. (2009)	Ol-phyric shergottite	~11	Filiberto and Dasgupta (2011)
	1297	Franz et al. (2014)			
RBT04261	1048	Franz et al. (2014)	Ol-phyric shergottite	38–52	Filiberto and Dasgupta (2011)
NWA2990	669	Franz et al. (2014)	Ol-phyric shergottite	1–2	Filiberto and Dasgupta (2011)
NWA5990	2433	Franz et al. (2014)	Ol-phyric shergottite	~16–29	Irving et al. (2010)
NWA5789	408	Franz et al. (2014)	Ol-phyric shergottite	0–1	Filiberto and Dasgupta (2011)
SaU005	1522	Franz et al. (2014)	Ol-phyric shergottite	~32–38	Filiberto and Dasgupta (2011)
Yamato 980459	560	Franz et al. (2014)	Ol-phyric shergottite	~3–7	Filiberto and Dasgupta (2011)
	1650 ± 320	Shirai and Ebihara (2004)			
Tissint	2053	Aoudjehane et al. (2012)	Ol-phyric shergottite	~8–24	Aoudjehane et al. (2012)
	1875	Franz et al. (2014)			
EET 79001A	2100 ± 700	Lodders (1998)	Ol-phyric shergottite	~17	McSween and Jarosewich (1983)
	1071	Franz et al. (2014)			
Nakhla	260 ± 80	Lodders (1998)	Nakhlite (clinopyroxenite)	~75–85	Treiman (2005)
Lafayette	420, 390	Gibson et al. (1985)	Nakhlite (clinopyroxenite)	~70–85	Treiman (2005)
NWA998	64	Franz et al. (2014)	Nakhlite (clinopyroxenite)	~85	Treiman (2005)
Y000593	34	Franz et al. (2014)	Nakhlite (clinopyroxenite)	~85	Shirai et al. (2002)
MIL03346	1287	Franz et al. (2014)	Nakhlite (clinopyroxenite)	~80	Day et al. (2006); Mikouchi et al. (2005)
MIL090030[c]	837	Franz et al. (2014)	Nakhlite (clinopyroxenite)		
MIL090032[c]	984	Franz et al. (2014)	Nakhlite (clinopyroxenite)		
MIL090136[c]	927	Franz et al. (2014)	Nakhlite (clinopyroxenite)		
NWA6148[c]	81	Franz et al. (2014)	Nakhlite (clinopyroxenite)		
LEW88516	950	Dreibus et al. (1992)	Lherzolitic shergottite	~87	Treiman et al. (1994)
ALH77005	510 ± 200	Lodders (1998)	Lherzolitic shergottite	~92	Papike et al. (2009)
	726	Franz et al. (2014)			
Chassigny	260 ± 130	Lodders (1998)	Dunite	~99	Floran et al. (1978)
	67	Franz et al. (2014)			
ALH84001	110 ± 10	Dreibus et al. (1994)	Orthopyroxenite	~98	Mittlefehldt (1994)
	103	Franz et al. (2014)			

[a] 1σ uncertainties of external reproducibility of replicates are given for this study and some of the previous studies (except Lodders, 1998; see below); External reproducibilities are not provided in Franz et al. (2014), but internal reproducibilities for single measurements are 2%; otherwise the uncertainties are not provided in the original studies.

[b] All the S concentration data from Lodders (1998) are average values summarized from different previous studies listed as follows: Shergotty – Gibson et al. (1985): 65, 330, 380, 2170 ppm; Burgess et al. (1989): 1950 ppm; Burghele et al. (1983): 1330 ppm; EET 79001B – McSween and Jarosewich (1983): 1784 ppm; Gibson et al. (1985): 1940 ppm; Banin et al. (1992), Burghele et al. (1983): 1600 ppm; EET 79001A – McSween and Jarosewich (1983): 2184 ppm; Gibson et al. (1985): 2540 ppm; Banin et al. (1992), Burghele et al. (1983): 1920 ppm; Nakhla – Burgess et al. (1989): 250 ppm, Gibson et al. (1985): 200, 260, 330, 360, 1040 ppm; Banin et al. (1992), Dreibus et al. (1982): 249 ppm; ALH 77005 – Burghele et al. (1983): 600 ppm; Burgess et al. (1989): 400 ppm; Banin et al. (1992): 600 ppm; Chassigny – Burgess et al. (1989): 250 ppm; Gibson et al. (1985): 300, 330, 360, 400 ppm; Banin et al. (1992), Dreibus et al. (1982): 118 ppm. The ± uncertainties in Lodders (1998) are calculated with respect to the mean value obtained from various studies.

[c] Major elements data/mineralogy of these four Nakhlites are not available.

plagioclase, oxide, sulfides, etc.) reported in previous studies and mineral densities. Possible maximum cumulus fraction in basaltic shergottites is approximated by weight percent of pyroxenes assuming pyroxenes are the only cumulus minerals, except for some meteorites (e.g., QUE94201). Cumulus fraction in ol-phyric shergottites cited is approximated by the proportion of excess olivine megacrysts. Cumulus fractions in nakhlites, lherzolites, chassignite and orthopyroxenite are calculated from mineral modes and densities. For the purpose of clarity, we refer extent of melting, F (in Fig. 5) to weight percent of melt produced by partial melting of the mantle.

3. Results

S concentration of the leachate was below the limit of detection (<20 ppm). Within the analytical errors, the two different fractions each from NWA 856, NWA 1068 and NWA 998 yielded identical results. Therefore, the S concentrations reported here for

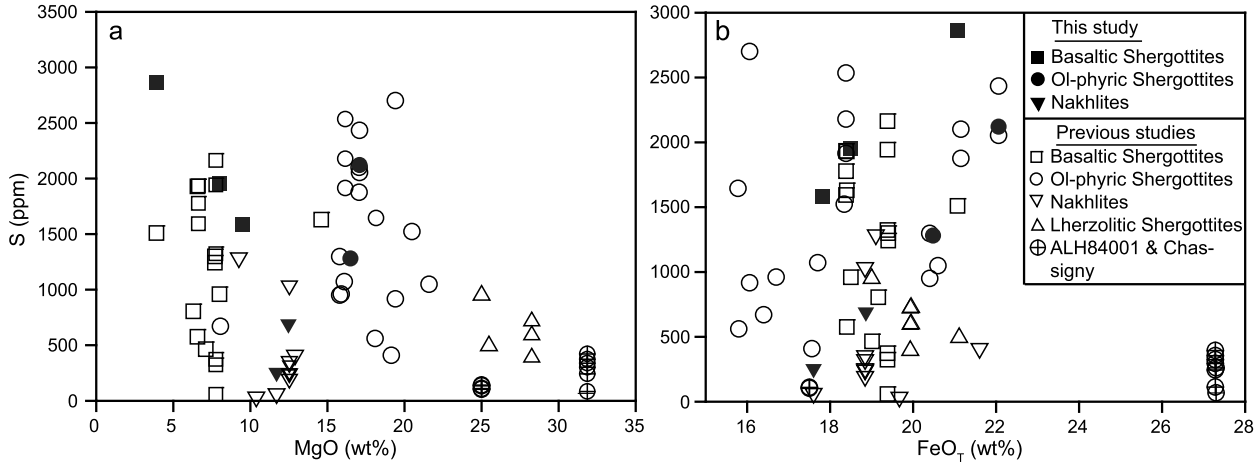

Fig. 1. Bulk S concentration of Martian meteorites versus (a) bulk MgO contents and (b) bulk FeO$_T$ contents. Bulk S contents of meteorites show weak to no correlation with bulk rock MgO and FeO$_T$ contents. (a) also shows that bulk S content of cumulate Martian meteorites (e.g., lherzolitic shergottites, ALH84001, Chassigny) cluster under 1000 ppm while basaltic shergottites and ol-phyric shergottites have a broader range of bulk S contents.

these samples are the averages of the data for the two different fractions for each meteorite. Basaltic shergottites Los Angeles, Zagami and NWA 856 have S contents of 2865 ± 224, 1954 ± 91 and 1584 ± 10 ppm, respectively. Olivine-phyric shergottites NWA 1068 and Tissint have S contents of 1280 ± 48 and 2120 ± 68 ppm. Clinopyroxenites Nakhla and NWA 998 yield the lowest S concentrations of 690 ± 60 and 253 ± 42 ppm S, respectively.

4. Discussion and implications

4.1. Comparison with previous bulk sulfur data of Martian meteorites

Our new measurements of shergottites' and nakhlites' bulk sulfur data fall in the range of bulk S from the previous studies (Banin et al., 1992; Burgess et al., 1989; Burghele et al., 1983; Dreibus et al., 1994, 1992, 1982; Franz et al., 2014; Gibson et al., 1985; Lodders, 1998; McSween and Jarosewich, 1983; Sarbadhikari et al., 2009; Zipfel et al., 2000). Sulfur concentrations of Los Angeles, Zagami, Nakhla and Tissint have been measured in previous studies (Aoudjehane et al., 2012; Banin et al., 1992; Burgess et al., 1989; Franz et al., 2014; Gibson et al., 1985; Dreibus et al., 1982). Sulfur concentrations in Tissint and Zagami from this study agrees well with those from previous studies (Aoudjehane et al., 2012; Gibson et al., 1985). However, bulk S concentrations of Los Angeles and Zagami from this study are both higher than the total S reported in Franz et al. (2014). Also bulk S concentration of Nakhla from this study is higher than most of the ones reported from previous studies (Banin et al., 1992; Burgess et al., 1989; Gibson et al., 1985). Whereas our bulk S concentration of Nakhla and NWA998 is within the range of nakhlites (34–1287 ppm) measured in previous studies (Banin et al., 1992; Burgess et al., 1989; Dreibus et al., 1982; Franz et al., 2014; Gibson et al., 1985). The variability in bulk S data on the same meteorite from different studies may reflect the heterogeneity in Martian meteorites (Burgess et al., 1989; McCoy et al., 1999; Warren et al., 2004). Thus, given relatively small aliquots of sample used in our and other previous measurements, it may not be surprising to obtain somewhat different bulk S values from different studies. Supplementary Table 1 shows that different total S concentration of a certain Martian meteorite reported in different studies is not unusual. In Fig. 2 all the meteorites with more than one S concentration measurement are identified. The difference among those measurements range from 20 to 800 ppm (Fig. 2; Table 1). Because the model proposed in this study is aimed at describing general behavior of S during fractional crystallization and partial melting on Mars, in

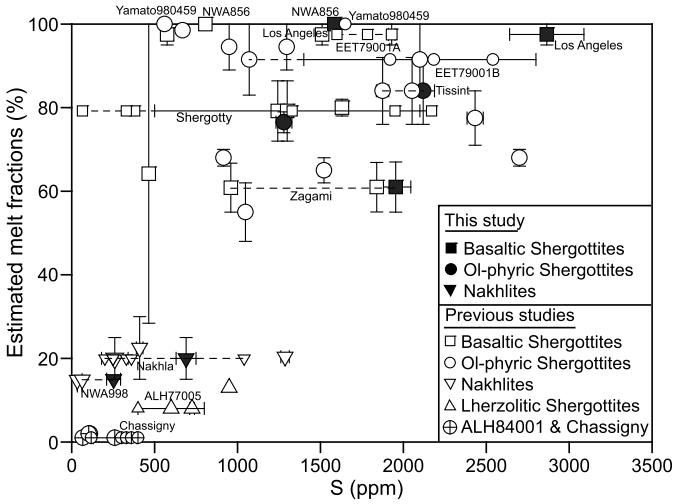

Fig. 2. Correlation between bulk S concentration of Martian meteorites and estimated fractions of melt trapped in various meteorites. Meteorites with more than one S concentration measurements by different studies are marked. Horizontal dashed lines connect different S concentration estimates of the same meteorites from various studies. Estimated trapped melt fractions and bulk S data plotted here are listed in Table 1.

Table 1 and the figures we reported all the S measurements for meteorites that have more than one measured results.

Bulk S data of Martian meteorites are plotted with their MgO concentrations in Fig. 1a. Because sulfur carrying capacity under relatively reduced conditions ($fO_2 <$ FMQ) is strongly related to FeO$_T$ concentration, we also plotted all S data with FeO$_T$ content of each meteorites in Fig. 1b. A lack of correlations between bulk sulfur contents of Martian meteorites and MgO or FeO$_T$ concentration in Fig. 1 suggests that neither pure fractional crystallization nor sulfide-saturation alone can explain the bulk S contents in most Martian meteorites. However, it is noticeable that bulk sulfur concentration of basaltic shergottites and ol-phyric shergottites show more scatter ranging from <500 ppm to >2500 ppm compared to those of cumulates (e.g., nakhlites, lherzolitic shergottites, and ALH84001), which mainly cluster at <1000 ppm (Fig. 1). As described in Section 2.2, it is recognized that most Martian meteorites are in fact not bonafide liquid compositions, but rather mixtures of liquids and cumulates, cognate xenoliths, antecrysts, etc., as is commonly seen on Earth. We noticed that basaltic shergottites and ol-phyric shergottites have relatively higher liquid

fractions (>60%) while cumulates contain <30% melt. Fig. 2 displays a correlation between bulk S concentrations for the Martian meteorites and the estimated fraction of liquid that the meteorites likely contain (Fig. 2; Table 1). The correlation suggests that the difference of bulk S concentration among different petrographic groups can result from different liquid–cumulus ratios during mixing. However, bulk S concentration variation within each group of Martian meteorite (e.g. basaltic shergottites and olivine-phyric shergottites) is less systematic (Fig. 2), which suggests that there may be other potential complexities shaping the sulfur inventory of Martian meteorites. In fact, assuming that secondary processes did not play a major role in shaping the bulk sulfur contents of Martian meteorites, the observed bulk S concentration is the product of a series of igneous processes: mantle melting, fractional crystallization, liquid–cumulus mixing and magmatic degassing. In the following sections, we will evaluate different igneous processes that potentially account for the S budgets of Martian meteorites.

4.2. *Modeling the fate of S during fractional crystallization of Martian magmas*

The observed correlation between estimated liquid fraction in each meteorite and the bulk sulfur content suggests that degassing of primary magma may not be the chief process affecting bulk sulfur contents of Martian meteorites. On the contrary cooling and crystallization of primary basalts may be important in explaining the trends seen in Fig. 2. Therefore it is critical to accurately model the evolution of S during fractional crystallization. Because S concentration in the silicate melt is always limited by the sulfur carrying capacity of the melt, one first needs to model how sulfur carrying capacity vary along the liquid line of descent (LLD) of a primary Martian basalt. Given the oxygen fugacity, fO_2 of Martian meteorites range from FMQ−5 to FMQ+0.46 (Goodrich, 2003; Herd, 2006; Herd et al., 2002; Karner et al., 2007; McCanta et al., 2004; Righter et al., 2008; Sautter et al., 2002; Shearer et al., 2006; Wadhwa, 2001), and because the transition from S^{2-} to S^{6+} in basaltic liquid occurs at $fO_2 \sim$ FMQ − FMQ+2 (Jugo, 2009; Jugo et al., 2010), the sulfur carrying capacity for primitive Martian magma must be represented by sulfur contents of basalts at sulfide saturation (SCSS). Basalt SCSS varies with pressure (P), temperature (T), fO_2, and melt composition and can be calculated using parameterizations from previous studies that aimed at constraining Martian basalt SCSS (Ding et al., 2014; Righter et al., 2009). We employed the parameterization from Ding et al. (2014) because this study modeled SCSS of Martian magmas based exclusively on high-FeO_T basalt experiments. The full method of the using alphaMELTS to calculate of the melt composition change along LLD, the choice of the starting liquid and fractional crystallization conditions are given in Supplementary Text. In addition, to avoid possible bias from alphaMELTS calculation in obtaining representative melt compositions along LLD, we also used the melt compositions from fractional crystallization experiments on Yamato980459 at 0.5 GPa by Rapp et al. (2013) (Supplementary Fig. 1).

Fig. 3 and Supplementary Fig. 1 show the variation of SCSS along LLD for various liquid compositions. According to our calculations, SCSS decreases along the LLD (thick solid lines in Fig. 3) at all conditions and for all compositions including the SCSS calculated from isobaric crystallization experiment by Rapp et al. (2013). One of the noticeable results of the model is that SCSS along LLD at 1 GPa is higher than that at 0.1 GPa. SCSS calculated from parameterizations from Righter et al. (2009) and Li and Ripley (2009) show the same trends, i.e., SCSS along LLD at 1 GPa is higher than that at 0.1 GPa (Supplementary Fig. 2). Although this may appear counter intuitive as SCSS increases with decreasing pressures (Ding et al., 2014; Holzheid and Grove, 2002), such dependence of SCSS on depth is only relevant for a constant melt composition and

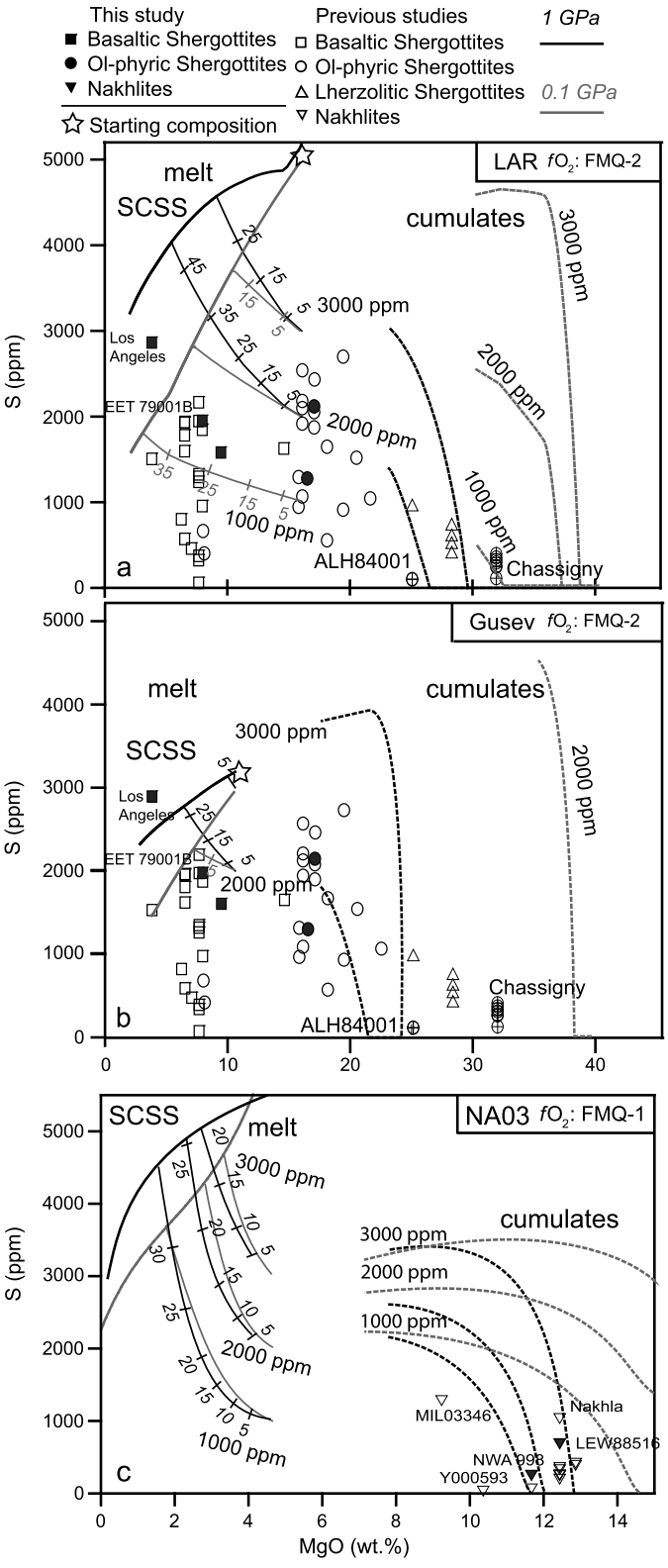

Fig. 3. Comparison of the bulk sulfur concentration (including data reported here and from previous studies) of Martian meteorites to the modeled sulfur concentration in derivative melts (solid lines) and cumulates (dashed lines) during isobaric fractional crystallization of compositions (a) LAR, (b) Gusev, and (c) NA03 (Supplementary Table 1). Thick solid lines indicate SCSS along LLD and intermediate-thickness solid curves with numbers represent liquids that are sulfide undersaturated (between 1000 and 3000 ppm S in the starting liquid) to begin with. Extent of fractional crystallization (in wt.%) is shown by tick marks along the intermediate solid curves with italic numbers. The grey and black curves represent calculation performed for 0.1 and 1.0 GPa, respectively.

at a constant temperature. However, there is also a broad agreement that increasing temperature and FeO_T concentration in the melt, especially the latter, enhance SCSS strongly because S^{2-} is bonded with Fe^{2+} in the silicate melt (Baker and Moretti, 2011; Ding et al., 2014; Liu et al., 2007; Mavrogenes and O'Neill, 1999). MELTS calculation shows that FeO_T increases strongly during isobaric fractional crystallization at 1 GPa while FeO_T slightly decreases or barely changes at 0.1 GPa. Results from crystallization experiments from low to high pressures show similar relations between FeO_T change during crystallization and pressure (Supplementary Fig. S3a). Therefore, higher FeO_T of derivative basalts during high pressure crystallization as well as higher liquidus temperature and higher temperature of crystallization interval (Supplementary Fig. 3b) suppress the pressure effect on SCSS and is responsible for higher SCSS at greater depth. Regardless of crystallization depth, because SCSS decreases along LLD, sulfide-saturated melt precipitates sulfide in cumulate assemblage along LLD (thick dotted lines in Fig. 3 and Supplementary Fig. 1). The concentration of sulfur in cumulates depends on (1) at what point during crystallization evolving melt reaches sulfide saturation and (2) how rapidly SCSS decreases with evolving melt composition and temperature. If the primitive magmas are sulfide-undersaturated, the more sulfur the melt starts out with, the earlier (at high temperature and smaller extent of crystallization) the melt becomes sulfide-saturated; the corresponding cumulates have higher sulfur contents for melts that are initially more S-rich. Our modeling (Fig. 3) also shows that SCSS of primitive or less evolved melt could be highly variable (5200 ppm vs. 3200 ppm) depending on melt composition, mainly FeO_T and MgO contents, which is a proxy of temperature (Supplementary Fig. 3b). SCSS of evolved melt at shallow depths of crystallization decreases sharply. Hence, low SCSS of remaining melt and highly sulfide-enriched cumulates are produced. The detailed description and explanation of S concentration change in various melts during crystallization are given in the Supplementary.

4.3. Bulk S of meteorites versus S of differentiating liquid

The evolution of S along LLD is compared to the bulk S of Martian meteorites in Fig. 3 and Supplementary Fig. 1 and possible scenarios of S evolution during fractional crystallization in the crust are shown in Fig. 4. Though most Martian meteorites plot below the SCSS lines, certain basaltic shergottites with low MgO contents between ~4 and 6 wt.% are at or close to the SCSS values obtained for shallow crystallization (Los Angeles and EET 79001B in Fig. 3a). With previous petrologic studies showing that both Los Angeles and EET 79001B are very close to a liquid composition (Righter et al., 2009; Rubin et al., 2000; Smith et al., 1984) it is reasonable to interpret their bulk S concentrations being similar to what the differentiated melts derived from Y98 or LAR at shallow depths would be at sulfide saturation. In this context, the match between the modeled SCSS and actual S contents suggests that at least some of the differentiated Martian basaltic magmas are sulfide-saturated without any S loss owing to degassing (liquid in scenario a and b in Fig. 4). The lack of S degassing could be result of several scenarios, such as that some Martian meteorites with cumulate textures may not be extrusive rocks (Hamilton et al., 2003); or oxygen fugacity is very low (Gaillard and Scaillet, 2009; Gaillard et al., 2012); or there is almost no CO_2 or H_2O in the melt to aid degassing (Gaillard and Scaillet, 2009; Gaillard et al., 2012). If degassing is not the chief process leading to lowering of S in the magmatic product, the bulk S concentration of such melt is the result of SCSS decrease during fractional crystallization. This is supported by the observation of rounded droplets and ellipsoidal blebs of sulfide grains in basaltic shergottites, suggesting solidification from immiscible sulfide melts from

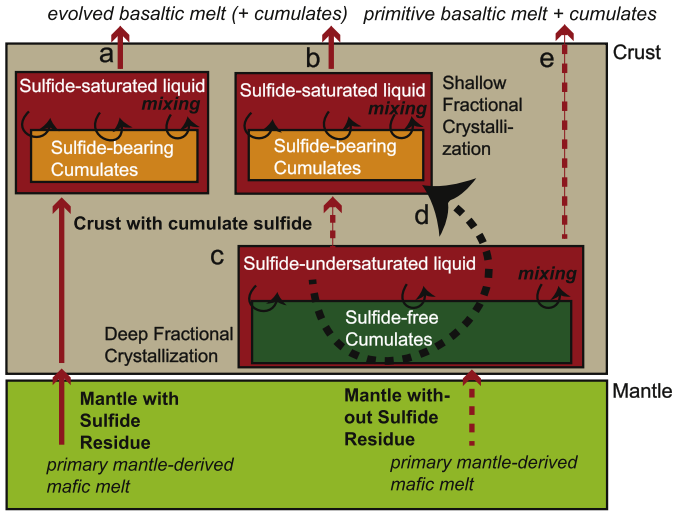

Fig. 4. Schematic diagram showing various scenarios of evolution of sulfur during emplacement and fractional crystallization of basalts in the crust. (a) Emplaced mantle-derived mafic melt is sulfide-saturated. Sulfide is enriched in the cumulates and evolved basaltic liquid is sulfide-saturated. (b) and (c) Emplaced mantle-derived mafic melt is not sulfide saturated. Regardless of the depth of crystallization, the cumulates are initially sulfide-free. Because S becomes enriched as an incompatible element in such a sulfide-undersaturated liquid, the liquid eventually becomes sulfide-saturated with sulfide-bearing cumulates. (d) Mixing between sulfide-free cumulates and sulfide-saturated liquid could be realized by magma chamber overturn in some open systems. (e) Sulfide-undersaturated liquid with or without some sulfide-free cumulates froze in before the melt becomes sulfide saturated. Output from sulfide-saturated liquid is represented by solid straight lines with arrows while that from sulfide-undersaturated liquid by dashed straight lines with arrows. Solid curved lines with arrows indicate liquid–cumulate mixing in a closed system while dashed curved line with arrow indicates liquid–cumulate mixing in an open system.

progressively more evolved silicate melts (Lorand et al., 2005). Furthermore, shallow crystallization condition also is in agreement with previous constraints on petrogenesis of basaltic shergottites (Hale et al., 1999; McCoy et al., 1992; Xirouchakis et al., 2002).

Comparison of bulk S concentration to plausible SCSS values at the same MgO contents for the rest of the available meteorites, however, show that the meteorite sulfur budgets are always lower than the predicted SCSS values. Righter et al. (2009) suggested that the deficit could be interpreted either as the S degassed from Martian magmas, or the melt is sulfide under-saturated and did not degas, or the melt is sulfide under-saturated, but the efficiency of S degassing of the melt is increased by the presence of water-rich vapor. SCSS is lowered by presence of vapor phase of other volatile such CO_2 and/or H_2O. In addition to these, given the correlation of bulk S with liquid fraction in Fig. 2 there are several alternative explanations of meteorite sulfur budgets related to the fact that most Martian meteorites are either basalts with significant admixing of cumulus minerals or cumulates with or without trapped interstitial liquids.

As discussed in Section 4.2, cumulates could be sulfide-free when the melt is sulfide undersaturated (cumulates in scenario c in Fig. 4) or sulfide-bearing (cumulates in scenario a and b in Fig. 4) when the evolving melt is sulfide saturated (two different primitive mafic melts in Fig. 4). Contributions from cumulates sulfides are likely represented by some cumulate Martian meteorites (e.g. nakhlites, lherzolitic shergottites, ALH84001 and Chassigny) with small proportions of trapped liquid (<5% for ALH84001 and Chassigny) whose bulk S concentrations match or are close to the modeled S contents in cumulates (Fig. 3—high pressure crystallization). The observations of minor amounts of poikilitic pyrrhotite in lherzolitic shergottite ALH77005 (Ikeda, 1994) and intergranular sulfide blebs in chassignite NWA 2737 (Lorand et al., 2012) support this model inference. Though petrogenesis of nakhlites have been

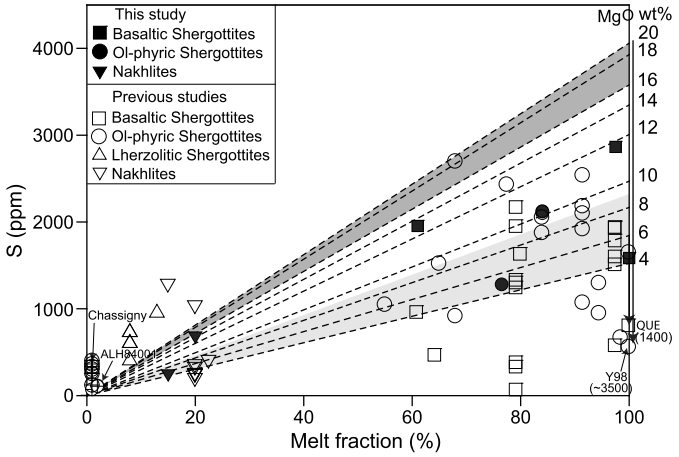

Fig. 5. Comparison of the bulk sulfur concentration of Martian meteorites from this study and other previous studies to the modeled sulfur concentration of meteorites by considering mixing between sulfide-saturated basaltic melt (at variable extent of fractional crystallization) and sulfide-free cumulates. Sulfur concentration at sulfide saturation (SCSS) here is calculated for melt compositions that derive from 0.1 GPa fractional crystallization of a primitive melt similar to Y98 at FMQ-2. SCSS model used is from Ding et al. (2014). Each dashed line represents bulk S concentration of meteorites that would result from entrapment of variable fractions of melt of different MgO content numbered at the right side of the figure in weight percent. When melt fraction is 100%, S concentration is equal to that of SCSS. Bulk S concentrations of the Martian meteorites are compared to the dashed lines with similar MgO contents. Light grey area defines possible bulk S concentration of basaltic shergottites while dark grey area defines the same for ol-phyric shergottites. The arrows and numbers in parentheses indicate the S deficit for QUE94201 or Yamato 980459 calling for either degassing or entrapment of sulfide under-saturated melt.

argued to be different from both Chassigny and shergottites (Jones, 1989; Treiman, 2005; Wadhwa and Crozaz, 1995), S contents in the nakhlites match very well with the modeled S concentration of cumulates crystallizing from a proposed nakhlites parental melt composition (Stockstill et al., 2005) at 1 GPa (Fig. 3c). This suggests that sulfide precipitation in the cumulates could be a common process during Martian magma evolution regardless the mantle source. It should be noted that the preferential occurrence of sulfides associated with interstitial minerals in nakhlites (Chevrier et al., 2011) argues the achievement of sulfide saturation at a late stage during magmatic differentiation. This scenario can only be satisfied by the model if the nakhlites parental melts started as being sulfide-undersaturated (Fig. 3c, Fig. 4 scenario c).

The rest of the meteorites, basaltic and Ol-phyric shergottites, contain small to moderate amount of cumulus minerals and their measured S contents are lower than the predicted SCSS values. There are several possibilities reconciling the deficit if volcanic degassing is not the chief mechanism for lower S content of the basaltic crust. Mixing between sulfide-saturated differentiated melts and equilibrium sulfide-bearing cumulates if primary magma is sulfide-undersaturated can regenerate bulk S contents of most basaltic and Ol-phyric shergottites (mixed output in scenario a or b in Fig. 4). However, this hypothesis contradicts the fact that no solitary sulfide inclusions in cumulus silicates (olivine, augite) in basaltic and Ol-phyric shergottites have been documented so far. It is more likely that sulfide in these shergottites originated from crystallization of a late stage, sulfide-saturated melt, based on their intimate intergrowth and positive correlation with modal Fe–Ti oxides (Lorand et al., 2005; McCoy et al., 1992; Xirouchakis et al., 2002). An alternate way to reproduce the S content in these basaltic and Ol-phyric shergottites is mixing between sulfide-saturated liquids or liquids with S concentration very close to SCSS and sulfide-free cumulus minerals. Interactions between sulfide saturated liquid and sulfide-free early cumulates can take place by open system magma chamber overturn (scenario d in Fig. 4). In this case, S is only contributed by sulfide-saturated melts and bulk S contents are related to SCSS of the melts and proportion of melts in the mixture (Fig. 5). In Fig. 5, each dashed line represents, certain MgO content of a single differentiating melt, bulk S of the mixture (sulfide-saturated melt + sulfide-free cumulus minerals) changes with changing melt fraction. Cumulate Martian meteorites (except two nakhlites) plot either on the dashed lines or above the lines. Cumulates sitting above the lines indicate extra S from cumulus minerals, which match the scenario of mixing between sulfide-bearing cumulus minerals and silicate melts proposed above. All the basaltic shergottites in the dataset have MgO contents less than 10 wt.%. The light grey area in Fig. 5 represents possible bulk S contents for mixing with each melt fraction. Bulk S contents of most basaltic shergottites (squares in Fig. 5) can be obtained in this way while certain amount of degassing is required for other basaltic shergottites. QUE94201 may be an example of degassed basaltic shergottites since it is thought to represent a relatively evolved (MgO ~6%) liquid composition (melt fraction equal to 100%) and 1400 ppm degassed S is needed to make up the deficit between bulk S and liquid SCSS (Fig. 5). The deficit is more common in ol-phyric shergottites. Dark grey area in Fig. 5 represents calculated S concentration of ol-phyric shergottites at different melt fractions, however, only one ol-phyric shergottite plots in that area. 160 to 3500 ppm degassing is required for ol-phyric shergottites in this model to lower the modeled bulk S contents to the measured values.

Another possible scenario is that primary magma of ol-phyric shergottites were sulfide undersaturated and these shergottitic liquid froze in before the melt becomes sulfide saturated (scenario e in Fig. 4). Therefore, bulk S contents in ol-phyric shergottites may result from either degassing or low initial S concentration (sulfide undersaturated) of the primary melt, or a combination of both. The scenario that primary magma is sulfide undersaturated is consistent with the low S contents (<1000 ppm) in the olivine-hosted melt inclusion in Yamato 980459 (Usui et al., 2012). Sulfide undersaturated primary magma can also limit the sulfide enrichment in the cumulates. Our model shows that once the melt is sulfide saturated, S concentration in the cumulates increases rapidly due to the dramatic decrease of SCSS. For example, by 30% fractional crystallization from Y98 at 1 GPa, S concentration in the cumulate can be as high as 4000 ppm (Supplementary Fig. 1). On the contrary S contents in cumulate Martian meteorites, irrespective of the class, mostly do not exceed 1000 ppm, suggesting that it is unlikely that primitive Martian magma start from sulfide-saturated condition. Therefore, in order to reproduce the sulfide saturated differentiated melt and precipitate realistic amount of sulfide in the cumulates, it is likely necessary that Martian mantle-derived primitive liquid was sulfide-undersaturated and became sulfide-saturated only during crystallization at a later stage.

4.4. S content in the primitive mantle-derived magma and S budget of the Martian mantle

If the parental basalts of Martian meteorites derive from sulfide-undersaturated primitive melts as discussed above, then the question becomes that how much sulfur does the mantle source regions of Martian mantle contain. By analogy to the fact that Earth's mantle is known to be sulfide saturated (Lorand, 1990; Lorand et al., 2013), one can assume that subsolidus Martian mantle is sulfide-saturated. This assumption is reasonable because Mars is thought to be a sulfur-rich planet (Dreibus and Wanke, 1985; Gaillard et al., 2012; King and McLennan, 2010) and oxygen fugacity of the Martian mantle is argued to be in the sulfide stability field (Jugo et al., 2010). The question is whether Martian mantle sulfide can survive during partial melting, which depends on extent of melting, SCSS of Martian mantle partial melts, and bulk S content of the mantle.

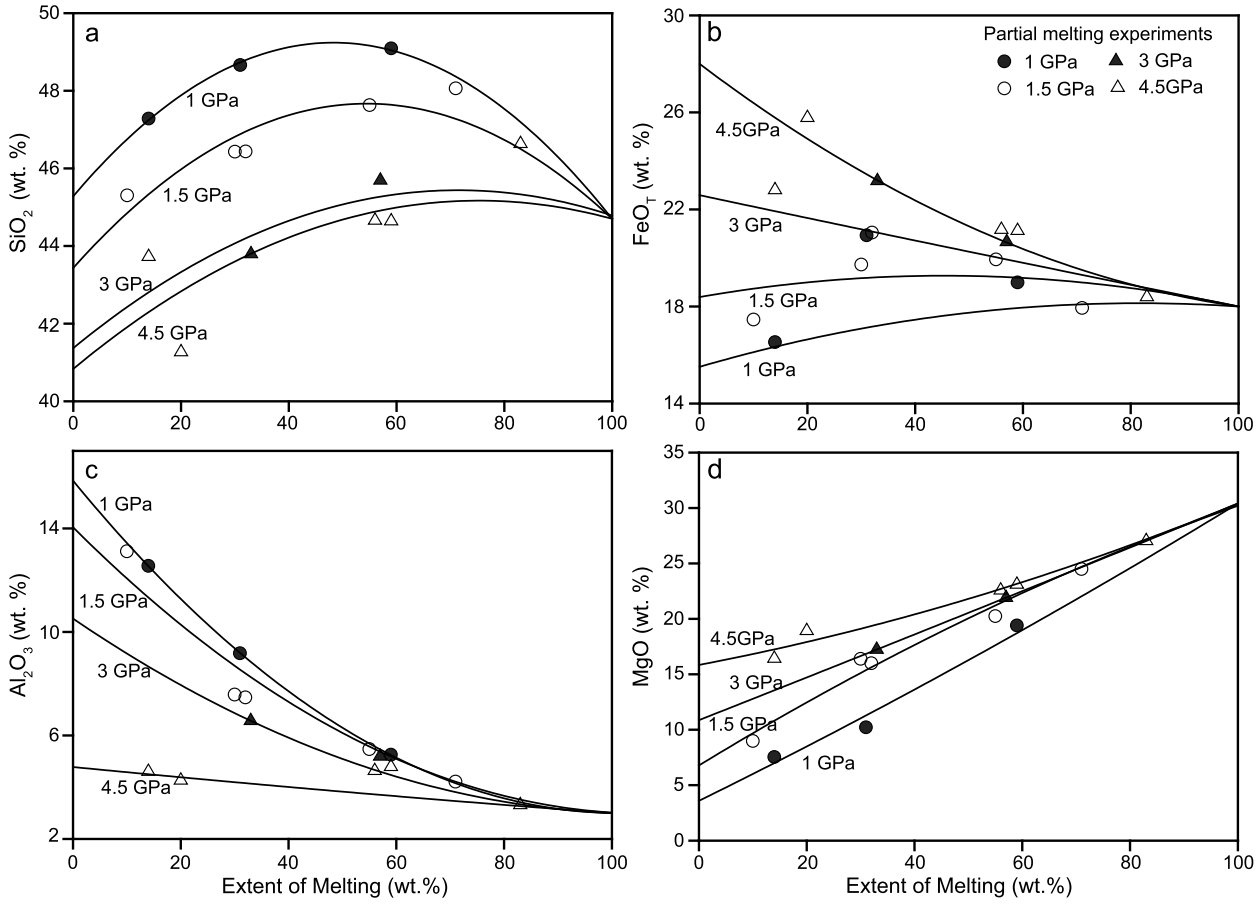

Fig. 6. (a) SiO_2, (b) FeO_T, (c) Al_2O_3, and (d) MgO concentration (wt.%) of the partial melt plotted as a function of increasing melting degree, F of Dreibus and Wanke (1985) model Martian mantle. Different symbols are experimental data at each pressure taken from Bertka and Holloway (1994) and Matsukage et al. (2013), and the solid lines are parameterization based on experimental data and starting compositions used in the experiments (when F = 100%, the concentration of each oxide equals that of the starting mantle composition).

To investigate the possibility of producing sulfide-undersaturated primitive magma, S contents of primary mantle-derived magmas are modeled from isentropic partial melting of model Martian mantle with mantle potential temperature of 1525 °C and 1365 °C, constrained by Filiberto and Dasgupta (2011). During isentropic decompression melting, extent of melting (F) increases with decreasing pressure (P), and we adopted the following equation (Eq. (1)) from Langmuir et al. (1992) to calculate the extent of melting with decreasing pressure.

$$\frac{dF}{dP} = \frac{(\frac{dT}{dP})_{adb} - (\frac{dT}{dP})_{sol}}{\frac{H_f}{C_P} + \frac{dT}{dF}}. \quad (1)$$

We use Martian mantle adiabatic gradient, $(\frac{dT}{dP})_{adb}$ of 0.18 °C/km, heat of fusion, H_f of 6.4×10^5 $JK^{-1}kg^{-1}$, and heat capacity, C_P of 1200 $JK^{-1}kg^{-1}$ (Kiefer, 2003). The slope of the solidus in P–T space, $(\frac{dT}{dP})_{sol}$ is from the parameterization of the Martian mantle solidus given by Filiberto and Dasgupta (2011). Extent of melting as a function of temperature at each pressure is approximated using isobaric partial melting experiments at 1.0, 1.5, 3.0, and 4.5 GPa on model Martian mantle (Bertka and Holloway, 1994; Matsukage et al., 2013). Melt composition change in each oxides with the increasing melting degree were also parameterized from the experimental data. Examples of SiO_2, FeO_T, Al_2O_3 and MgO change (X) with increasing degree of melting (F) at each pressure are shown in Fig. 6. Combining $(\frac{dF}{dP})$ and $(\frac{dX}{dF})_P$, we constrained the melt composition change along decompression melting adiabat. The examples of SiO_2, FeO_T, Al_2O_3 and MgO change during decompression melting of the hot mantle are shown in Fig. 7b while Fig. 7a is the P–T diagram showing the framework of isentropic melting both for hot and cold mantle.

With the knowledge of the P, T and composition change along the decompression melting of both hot and cold mantle (Fig. 7), we calculated SCSS and S profile in the partial melts during adiabatic decompression melting. With the presence of sulfide in the mantle, at any given step of the melting process, $C_{l,i+1} = C_{SCSS,i}$. The concentration of S in the solid Martian mantle residue ($C_{r,i+1}$) is

$$C_{r,i+1} = \frac{M_i C_{r,i} - C_{scss,i}\Delta M}{M_{i+1}} \quad (2)$$

where M_i is the mass of the solid residue step i and $\Delta M = M_i - M_{i+1}$ is the change in mass of the solid residue. After the exhaustion of sulfide, $C_{r,i}$ becomes 0 and S concentration of the melt decreases by dilution with increasing degree of melting.

During decompression melting, SCSS decreases rapidly from >8000 ppm to ~3000 ppm if the mantle is hot (black thick solid line in Fig. 8a) while from ~5000 ppm to ~2000 ppm for cold mantle (grey thick solid line in Fig. 8b). This decreasing trend is mainly influenced by the FeO_T concentration decrease in the melt from higher T of melting at greater depths to cooler temperature of melt adiabat at shallower depths (Fig. 7). SCSS along the melting adiabat calculated using the SCSS parameterization of Righter et al. (2009), represented by thick dashed lines, also yields a similar trend. The thick dotted lines, representing SCSS along the melting adiabat with a fixed composition (Y98 from Greshake et al., 2004) have steeper slopes than the others. The difference between

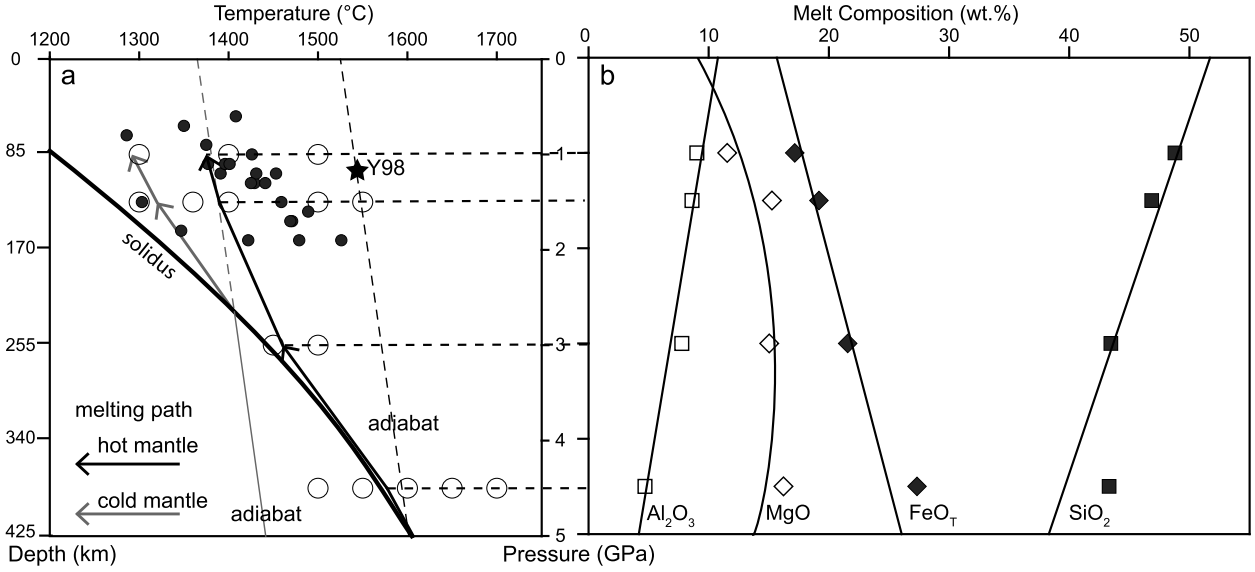

Fig. 7. (a) A pressure–temperature plot showing the framework of decompression melting of the Martian mantle with $T_P = 1525\,^{\circ}C$ (hot mantle) and $T_P = 1365\,^{\circ}C$ (cold mantle). Thin solid lines with arrows are melting adiabats applicable for these two mantle potential temperatures. The Martian mantle solidus is from Filiberto and Dasgupta (2011). Open circles indicate the P–T conditions of the partial melting experiments from Bertka and Holloway (1994) at 1.5 GPa and Matsukage et al. (2013) at 1.0, 3.0 and 4.5 GPa that constrain evolution of partial melt compositions with depth and temperature. Filled circles represent P–T conditions of Martian surface basalts in equilibrium with their mantle source (Filiberto and Dasgupta, 2011). Filled star represents the plausible condition of melt-mantle equilibration for Y98 (Musselwhite et al., 2006). (b) Estimated change of partial melt compositions along the hot melting adiabat based on experiments of Matsukage et al. (2013) and Bertka and Holloway (1994).

SCSS of a basalt of fixed composition and those that are produced by progressive melting suggests that composition change during partial melting can have a big influence on SCSS, hence the S behavior in the melt. Thin solid lines in Fig. 8 indicate the S dilution profile in the melts after mantle sulfide is exhausted. The point at which mantle sulfide is exhausted depends on initial storage of S in the mantle. For example, in Fig. 8a, Martian mantle containing 200 ppm S would exhaust all sulfides by 2% partial melting and a mantle containing 1000 ppm S by 12% partial melting. Within the plausible melting degree of Martian meteorites estimated by previous studies (Agee and Draper, 2004; Kiefer, 2003; Musselwhite et al., 2006, ~17% melting degree; light grey box in Fig. 8a and 8b), a hot Martian mantle can contain no more than 1000 ppm S in order to produce sulfide undersaturated primitive magmas. S behavior is similar in the cold mantle, although because of lower temperatures, SCSS in the cold mantle is generally much lower than that in the hot mantle. Fig. 8b shows that 700 ppm S is the upper limit to derive sulfide undersaturated primitive magmas within 17% melting degree from a relatively cold mantle.

One important fact is that the constraints above for the plausible sulfur abundance of Martian meteorite source regions derive entirely from the bulk S data of Martian meteorites and the experimental constraints on sulfur storage capacity of Martian magma. Although, <700–1000 ppm S for the Martian mantle is lower compared to some literature estimates (700–2000 ppm S; Gaillard et al., 2012), the range is still consistent with the expected abundance of mantle S based on physical properties of bulk Mars and the equilibrium core–mantle partitioning during magma ocean stage (Dreibus and Wanke, 1985; Lodders and Fegley, 1997; Sanloup et al., 1999). However, it cannot be ruled out that the Martian mantle sulfur budget was higher than the 700–1000 ppm range in the past, i.e., during the Noachian and early Hesperian. Given the relatively young age of the analyzed Martian meteorites (<500 Ma) and the possible lack of crustal recycling on Mars (McSween et al., 2009; Morschhauser et al., 2011), S budget of the Martian mantle might have been higher in the past and diminishing with time. It is still therefore possible that voluminous volcanism during early Mars produced sulfide-saturated primitive basalts with sulfide remaining in the residue of mantle melting. ~3500 ppm S loss from Yamato 980459, a primary melt composition (Fig. 5), may be an indication of the possible magnitude of S released from sulfide-saturated Martian basalts. On the other hand, if the Martian meteorite sulfur data are any indication of the sulfur budget of ancient (3.7–4.3 Ga) Martian crust, S-degassing to the late Noachian and early Hesperian atmosphere could also be limited; instead, cumulates in the Martian crust could be an important inventory of magmatic sulfur as it may also be on Earth (Lee et al., 2012).

5. Conclusions

We measured bulk S concentration of 7 Martian meteorites (2 olivine-phyric shergottites, 3 basaltic shergottites, and 2 nakhlites). Comparisons between all currently available bulk S data of Martian meteorites and the estimated melt fraction that they may contain suggest that the bulk S contents of Martian meteorites could be product of magma fractional crystallization and cumulate–melt mixing. Our model does not rule out sulfur degassing, but calls for caution in the estimation of the amount of S outgassing via young Martian basaltic volcanism. If meteorite sulfur data are any indication of the sulfur budget of ancient Martian crust, S-degassing to the late Noachian and early Hesperian atmosphere could also be limited; instead, cumulates in the deep root of Martian crust could be an important inventory of magmatic sulfur (Lee et al., 2012).

Our modeling also shows that cumulates could be highly S enriched during fractional crystallization once the melt is sulfide saturated. The earlier the melt is sulfide saturated, the higher are S contents in the cumulates. Because most cumulate-bearing meteorites including olivine-phyric shergottites and lherzolitic shergottites have low S concentration, it is likely that primitive Martian magmas are sulfide-undersaturated and become sulfide saturated only at a later stage along liquid line of descent. In order to derive such sulfide-undersaturated primitive magma by adiabatic decompression melting, S content of the mantle source of Martian meteorites should be as low as ≤700–1000 ppm, which overlaps with the lower end of the previous estimated range of 700–2000 ppm S (Gaillard et al., 2012).

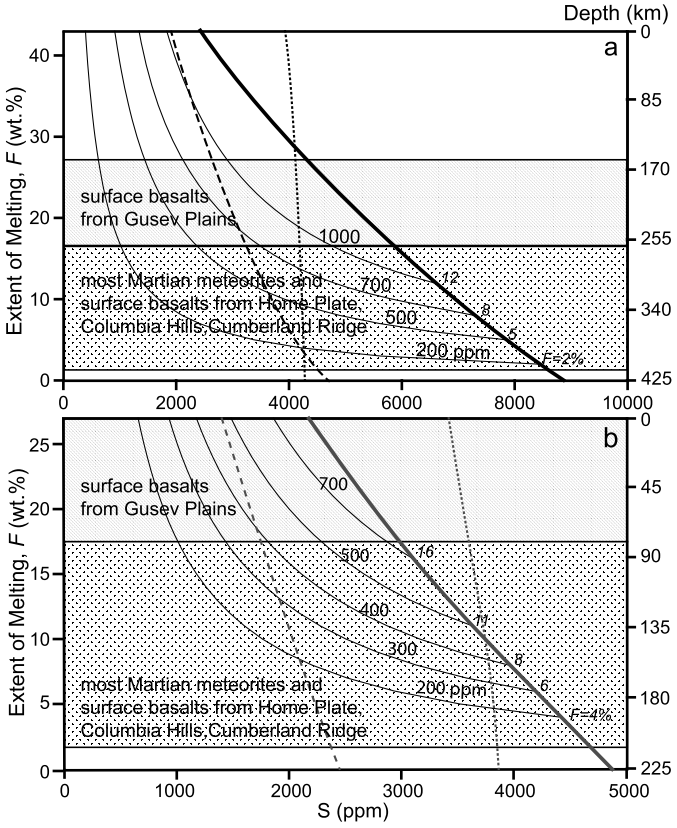

Fig. 8. S concentration in the melt (in ppm) versus melt fraction (F) and depth during isentropic batch melting of a model Martian mantle for (a) hot mantle (T_P = 1525 °C) and (b) cold mantle (T_P = 1365 °C). Thick solid line indicates SCSS change during decompressing melting (for calculation see text and Fig. 7). Thick dashed line represents SCSS along the melting adiabat calculated using the SCSS parameterization of Righter et al. (2009). Thick dotted line shows SCSS along the melting adiabat with fixed composition of Y98 from Greshake et al. (2004). Thin curves represent dilution of melt sulfur content after the consumption of residual sulfide for bulk Martian mantle with different S content ranging from 200 to 1000 ppm. Italicized numbers next to the SCSS lines in both (a) and (b) indicate the melting degrees at which sulfide is consumed for a mantle with certain amount of S. Also included (horizontal bands) for reference are plausible melt fractions that the Martian meteorites and different surface basalts may represent (e.g. Agee and Draper, 2004; Filiberto and Dasgupta, 2011; Kiefer, 2003; Musselwhite et al., 2006).

Acknowledgements

This article benefited from thorough and thoughtful formal reviews by Fabrice Gaillard and two anonymous referees. This work received support by a NASA grant NNX13AM51G and a Packard fellowship for science and engineering to R. Dasgupta. C.-T. A. Lee received support from NSF grant EAR 1347085.

Appendix A. Supplementary material

Supplementary material related to this article can be found online at http://dx.doi.org/10.1016/j.epsl.2014.10.046.

References

Agee, C.B., Draper, D.S., 2004. Experimental constraints on the origin of Martian meteorites and the composition of the Martian mantle. Earth Planet. Sci. Lett. 224, 415–429.
Aoudjehane, H.C., Avice, G., Barrat, J., Boudouma, O., Chen, G., Duke, M.J.M., Franchi, I.A., Gattacceca, J., Grady, M.M., Greenwood, R.C., Herd, C.D.K., Hewins, R., Jambon, A., Marty, B., Rochette, P., Smith, C.L., Sautter, V., Verchovsky, A., Weber, P., Zanda, B., 2012. Tissint martian meteorite: a fresh look at the interior, surface, and atmosphere of Mars. Science 338, 785–788.
Baker, D.R., Moretti, R., 2011. Modeling the solubility of sulfur in magmas: a 50-year old geochemical challenge. Rev. Mineral. Geochem. 73, 167–213.
Banin, A., Clark, B., Wänke, H., 1992. Surface Chemistry and Mineralogy. Mars.
Bertka, C.M., Holloway, J.R., 1994. Anhydrous partial melting of an iron-rich mantle II: primary melt compositions at 15 kbar. Contrib. Mineral. Petrol. 115, 323–338.
Burgess, R., Wright, I.P., Pillinger, C.T., 1989. Distribution of sulphides and oxidised sulphur components in SNC meteorites. Earth Planet. Sci. Lett. 93, 314–320.
Burghele, A., Dreibus, G., Palme, H., Rammensee, W., Spettel, B., Weckwerth, G., Wanke, H., 1983. Chemistry of shergottites and the Shergotty parent body (SPB): further evidence for the two component model of planet formation. Lunar Planet. Inst. Sci. Conf. 14, 80–81.
Chevrier, V., Lorand, J.-P., Sautter, V., 2011. Sulfide petrology of four nakhlites: Northwest Africa 817, Northwest Africa 998, Nakhla, and Governador Valadares. Meteorit. Planet. Sci. 46, 769–784.
Day, J., Taylor, L., Floss, C., McSween, H.Y., 2006. Petrology and chemistry of MIL 03346 and its significance in understanding the petrogenesis of nakhlites on Mars. Meteorit. Planet. Sci. 41, 581–606.
Ding, S., Dasgupta, R., Tsuno, K., 2014. Sulfur concentration of martian basalts at sulfide saturation at high pressures and temperatures – implications for deep sulfur cycle on Mars. Geochim. Cosmochim. Acta 131, 227–246.
Dreibus, G., Burghele, A., Jochum, K., Spettel, B., Wlotzka, F., Wanke, H., 1994. Chemical and mineral composition of ALH 84001: a Martian orthopyroxenite. Meteoritics 29, 461.
Dreibus, G., Jochum, K., Palme, H., Spettel, B., Wlotzka, F., Wanke, H., 1992. LEW 88516: a meteorite compositionally close to the "Martian mantle". Meteoritics 27, 216.
Dreibus, G., Palme, H., Rammensee, W., Spettel, B., Wechwerth, G., Wanke, H., 1982. Composition of Shergotty parent body: further evidence for a two component model of planet formation. Lunar Planet. Inst. Sci. Conf. Abstr. 13, 186–187.
Dreibus, G., Wanke, H., 1985. Mars, a volatile-rich planet. Meteoritics 20, 367–381.
Erdman, M.E., Lee, C.-T.A., Yang, W., Ingram, L., 2014. Sulfur concentration in geochemical reference materials by solution inductively coupled plasma-mass spectrometry. Geostand. Geoanal. Res. 38, 51–60.
Filiberto, J., Dasgupta, R., 2011. Fe^{2+}–Mg partitioning between olivine and basaltic melts: applications to genesis of olivine-phyric shergottites and conditions of melting in the Martian interior. Earth Planet. Sci. Lett. 304, 527–537.
Floran, R.J., Prinz, M., Hlava, P.F., Keil, K., Nehru, C.E., Hinthorne, J.R., 1978. The Chassigny meteorite: a cumulate dunite with hydrous amphibole-bearing melt inclusions. Geochim. Cosmochim. Acta 42, 1213–1229.
Franz, H.B., Kim, S.-T., Farquhar, J., Day, J.M.D., Economos, R.C., McKeegan, K.D., Schmitt, A.K., Irving, A.J., Hoek, J., Dottin, J., 2014. Isotopic links between atmospheric chemistry and the deep sulphur cycle on Mars. Nature 508, 364–368.
Gaillard, F., Michalski, J., Berger, G., McLennan, S.M., Scaillet, B., 2012. Geochemical reservoirs and timing of sulfur cycling on Mars. Space Sci. Rev. 174, 251–300.
Gaillard, F., Scaillet, B., 2009. The sulfur content of volcanic gases on Mars. Earth Planet. Sci. Lett. 279, 34–43.
Gibson, E.K., Moore, C.B., Primus, T.M., Lewis, C.F., 1985. Sulfur in achondritic meteorites. Meteoritics 20, 503–511.
Goodrich, C.A., 2002. Olivine-phyric martian basalts: a new type of shergottite. Meteorit. Planet. Sci. 37, B31–B34.
Goodrich, C.A., 2003. Petrogenesis of olivine-phyric shergottites Sayh al Uhaymir 005 and Elephant Moraine A79001 lithology A. Geochim. Cosmochim. Acta 67, 3735–3772.
Greshake, A., Fritz, J., Stöffler, D., 2004. Petrology and shock metamorphism of the olivine-phyric shergottite Yamato 980459. Geochim. Cosmochim. Acta 68, 2359–2377.
Hale, V.P., McSween, H.Y., McKay, G.A., 1999. Re-evaluation of intercumulus liquid composition and oxidation state for Shergotty meteorite. Geochim. Cosmoschim. Acta 63, 1459–1470.
Halevy, I., Zuber, M.T., Schrag, D.P., 2007. A sulfur dioxide climate feedback on early Mars. Science 318, 1903–1907.
Hamilton, V.E., Christensen, P.R., McSween, H.Y., Bandfield, J.L., 2003. Searching for the source regions of martian meteorites using MGS TES: integrating martian meteorites into the global distribution of igneous materials on Mars. Meteorit. Planet. Sci. 38, 871–885.
Herd, C.D.K., 2006. Insights into the redox history of the NWA 1068/1110 martian basalt from mineral equilibria and vanadium oxybarometry. Am. Mineral. 91, 1616–1627.
Herd, C.D., Borg, L.E., Jones, J.H., Papike, J.J., 2002. Oxygen fugacity and geochemical variations in the martian basalts: implications for martian basalt petrogenesis and the oxidation state of the upper mantle of Mars. Geochim. Cosmochim. Acta 66, 2025–2036.
Holzheid, A., Grove, T.L., 2002. Sulfur saturation limits in silicate melts and their implications for core formation scenarios for terrestrial planets. Am. Mineral. 87, 227–237.
Hui, H., Peslier, A.H., Lapen, T.J., Shafer, J.T., Brandon, A.D., Irving, A.J., 2011. Petrogenesis of basaltic shergottite Northwest Africa 5298: closed-system crystallization of an oxidized mafic melt. Meteorit. Planet. Sci. 46, 1313–1328.
Ikeda, Y., 1994. Petrography and petrology of the ALH-77005 shergottite. Proc. NIPR Symp. Antarct. Meteor. 7, 9–29.
Irving, A.J., Kuehner, S.M., Herd, C.D.K., Gellissen, M., Rumble, D., Lapen, T.J., Ralew, S., Altmann, M., 2010. Olivine-bearing diabasic shergottite Northwest Africa

5990: petrology and composition of a new type of depleted martian igneous rock. Lunar Planet. Sci. Conf. 41, 1833.
Jégo, S., Dasgupta, R., 2013. Fluid-present melting of sulfide-bearing ocean-crust: experimental constraints on the transport of sulfur from subducting slab to mantle wedge. Geochim. Cosmochim. Acta 110, 106–134.
Jégo, S., Dasgupta, R., 2014. The fate of sulfur during fluid-present melting of subducting basaltic crust at variable oxygen fugacity. J. Petrol. 55, 1019–1050.
Johnson, S.S., Mischna, M.A., Grove, T.L., Zuber, M.T., 2008. Sulfur-induced greenhouse warming on early Mars. J. Geophys. Res. 113, E08005.
Jones, J., 1989. Isotopic relationships among the shergottites, the nakhlites and Chassigny. Lunar Planet. Sci. Conf. 19, 465–474.
Jugo, P.J., 2009. Sulfur content at sulfide saturation in oxidized magmas. Geology 37, 415–418.
Jugo, P.J., Wilke, M., Botcharnikov, R.E., 2010. Sulfur K-edge XANES analysis of natural and synthetic basaltic glasses: implications for S speciation and S content as function of oxygen fugacity. Geochim. Cosmochim. Acta 74, 5926–5938.
Karner, J., Papike, J., Shearer, C.K., McKay, G., Le, L., Burger, P., 2007. Valence state partitioning of Cr and V between pyroxene-melt: estimates of oxygen fugacity for martian basalt QUE 94201. Am. Mineral. 92, 1238–1241.
Kiefer, W.S., 2003. Melting in the martian mantle: shergottite formation and implications for present-day mantle convection on Mars. Meteorit. Planet. Sci. 38, 1815–1832.
King, P.L., McLennan, S.M., 2010. Sulfur on Mars. Elements 6, 107–112.
Langmuir, C.H., Klein, E.M., Plank, T., 1992. Petrological systematics of mid-ocean ridge basalts: constraints on melt generation beneath ocean ridges [WWW Document]. In: Morgan, J.P., Blackman, D.K., Sint, J.M. (Eds.), Mantle Flow Melt Gener. Mid-Ocean Ridges. In: Geophys. Monogr. Ser., vol. 71.
Lee, C.-T.A., Luffi, P., Chin, E.J., Bouchet, R., Dasgupta, R., Morton, D.M., Le Roux, V., Yin, Q.-Z., Jin, D., 2012. Copper systematics in arc magmas and implications for crust–mantle differentiation. Science 80 (336), 64–68.
Li, C., Ripley, E.M., 2009. Sulfur contents at sulfide-liquid or anhydrite saturation in silicate melts: empirical equations and example applications. Econ. Geol. 104, 405–412.
Liu, Y., Samaha, N., Baker, D.R., 2007. Sulfur concentration at sulfide saturation (SCSS) in magmatic silicate melts. Geochim. Cosmochim. Acta 71, 1783–1799.
Lodders, K., 1998. A survey of shergottite, nakhlite and chassigny meteorites whole-rock compositions. Meteorit. Planet. Sci. 33, A183–A190.
Lodders, K., Fegley Jr., B., 1997. An oxygen isotope model for the composition of Mars. Icarus 126, 373–394.
Lorand, J., 1990. Are spinel lherzolite xenoliths representative of the abundance of sulfur in the upper mantle? Geochim. Cosmochim. Acta 54, 1487–1492.
Lorand, J.-P., Chevrier, V., Sautter, V., 2005. Sulfide mineralogy and redox conditions in some shergottites. Meteorit. Planet. Sci. 40, 1257–1272.
Lorand, J.-P., Jean-Alix, B., Chevrier, V., Sautter, V., Pont, S., 2012. Metal-saturated sulfide assemblages in NWA 2737: evidence for impact-related sulfur devolatilization in Martian meteorites. Meteorit. Planet. Sci. 47, 1830–1841.
Lorand, J.-P., Luguet, A., Alard, O., 2013. Platinum-group element systematics and petrogenetic processing of the continental upper mantle: a review. Lithos 164–167, 2–21.
Matsukage, K.N., Nagayo, Y., Whitaker, M.L., Takahashi, E., Kawasaki, T., 2013. Melting of the Martian mantle from 1.0 to 4.5 GPa. J. Mineral. Petrol. Sci. 108, 201–214.
Mavrogenes, J.A., O'Neill, H.S., 1999. The relative effects of pressure, temperature and oxygen fugacity on the solubility of sulfide in mafic magmas. Geochim. Cosmochim. Acta 63, 1173–1180.
McCanta, M.C., Rutherford, M.J., Jones, J.H., 2004. An experimental study of rare earth element partitioning between a shergottite melt and pigeonite: implications for the oxygen fugacity of the martian interior. Geochim. Cosmochim. Acta 68, 1943–1952.
McCoy, T., Wadhwa, M., Keil, K., 1999. New lithologies in the Zagami meteorite: evidence for fractional crystallization of a single magma unit on Mars. Geochim. Cosmochim. Acta 63, 1249–1262.
McCoy, T.J., Taylor, G.J., Keil, K., 1992. Zagami: product of a two-stage magmatic history. Geochim. Cosmochim. Acta 56, 3571–3582.
McSween, H., Taylor, G., Wyatt, M., 2009. Elemental composition of the Martian crust. Science 80 (324), 736–739.
McSween, H.Y., Eisenhour, D.D., Taylor, L.A., Wadhwa, M., Crozaz, G., 1996. QUE94201 shergottite: crystallization of a Martian basaltic magma. Geochim. Cosmochim. Acta 60, 4563–4569.
McSween, H.Y., Jarosewich, E., 1983. Petrogenesis of the Elephant Moraine A79001 meteorite: multiple magma pulses on the shergottite parent body. Geochim. Cosmochim. Acta 47, 1501–1513.
Mikouchi, T., Monkawa, A., Koizumi, E., Chokai, J., Miyamoto, M., 2005. MIL03346 Nakhlite and NWA2737. Annu. Lunar Planet. Sci. Conf. 36, 1944.
Mittlefehldt, D.W., 1994. ALH84001, a cumulate orthopyroxenite member of the martian meteorite clan. Meteoritics 29, 214–221.
Morschhauser, A., Grott, M., Breuer, D., 2011. Crustal recycling, mantle dehydration, and the thermal evolution of Mars. Icarus 212, 541–558.
Musselwhite, D.S., Dalton, H.A., Kiefer, W.S., Treiman, A.H., 2006. Experimental petrology of the basaltic shergottite Yamato-980459: implications for the thermal structure of the Martian mantle. Meteorit. Planet. Sci. 41, 1271–1290.
Papike, J.J., Karner, J.M., Shearer, C.K., Burger, P.V., 2009. Silicate mineralogy of martian meteorites. Geochim. Cosmochim. Acta 73, 7443–7485.
Rapp, J.F., Draper, D.S., Mercer, C.M., 2013. Anhydrous liquid line of descent of Yamato-980459 and evolution of Martian parental magmas. Meteorit. Planet. Sci. 48, 1780–1799.
Righter, K., Pando, K., Danielson, L.R., 2009. Experimental evidence for sulfur-rich martian magmas: implications for volcanism and surficial sulfur sources. Earth Planet. Sci. Lett. 288, 235–243.
Righter, K., Yang, H., Costin, G., Downs, R.T., 2008. Oxygen fugacity in the Martian mantle controlled by carbon: new constraints from the nakhlite MIL 03346. Meteorit. Planet. Sci. 43, 1709–1723.
Rubin, A.E., Warren, P.H., Greenwood, J.P., Verish, R.S., Leshin, L.A., Hervig, R.L., Clayton, R.N., Mayeda, T.K., 2000. Los Angeles: the most differentiated basaltic martian meteorite. Geology 28, 1011–1014.
Sanloup, C., Jambon, A., Gillet, P., 1999. A simple chondritic model of Mars. Phys. Earth Planet. Inter. 112, 43–54.
Sarbadhikari, A.B., Day, J.M.D., Liu, Y., Rumble, D., Taylor, L.A., 2009. Petrogenesis of olivine-phyric shergottite Larkman Nunatak 06319: implications for enriched components in Martian basalts. Geochim. Cosmochim. Acta 73, 2190–2214.
Sautter, V., Barrat, J., Jambon, A., Lorand, J., Gillet, P.H., Javoy, M., Joron, J., Lesourd, M., 2002. A new Martian meteorite from Morocco: the nakhlite North West Africa 817. Earth Planet. Sci. Lett. 195, 223–238.
Self, S., Blake, S., Sharma, K., Widdowson, M., Sephton, S., 2008. Sulfur and chlorine in late Cretaceous Deccan magmas and eruptive gas release. Science 319, 1654–1657.
Shearer, C.K., McKay, G., Papike, J.J., Karner, J.M., 2006. Valence state partitioning of vanadium between olivine-liquid: estimates of the oxygen fugacity of Y980459 and application to other olivine-phyric martian basalts. Am. Mineral. 91, 1657–1663.
Shirai, N., Ebihara, M., 2004. Chemical characteristics of a Martian meteorite, Yamato 980459. Antarct. Meteor. Res. 17, 55.
Shirai, N., Oura, Y., Ebihara, M., 2002. Chemical composition of newly collected antarctic nakhlites, Y000593 and Y000749. In: Unmixing the SNCs: Chemical, Isotopic, and Petrologic Components of the Martian Meteorites, LPI Contribution No. 1134, pp. 55–56.
Smith, M.R., Laul, J.C., Ma, M.S., Huston, T., Verkouteren, R.M., Lipschutz, M.E., Schmitt, R.A., 1984. Petrogenesis of the SNC (shergottites, nakhlites, chassignites) meteorites: implications for their origin from a large dynamic planet, possibly Mars. J. Geophys. Res. 89, B612–B630.
Stewart, A.J., Schmidt, M.W., van Westrenen, W., Liebske, C., 2007. Mars: a new core-crystallization regime. Science 316, 1323–1325.
Stockstill, K.R., McSween, H.Y., Bodnar, R.J., 2005. Melt inclusions in augite of the Nakhla martian meteorite: evidence for basaltic parental melt. Meteorit. Planet. Sci. 40, 377–396.
Stolper, E., McSween, H.Y., 1979. Petrology and origin of the shergottite meteorites. Geochim. Cosmochim. Acta 43, 1475–1498.
Symes, S.J.K., Borg, L.E., Shearer, C.K., Irving, A.J., 2008. The age of the martian meteorite Northwest Africa 1195 and the differentiation history of the shergottites. Geochim. Cosmochim. Acta 72, 1696–1710.
Treiman, A.H., 2005. The nakhlite meteorites: augite-rich igneous rocks from Mars. Chem. Erde 65, 203–270.
Treiman, A.H., McKay, G.A., Bogard, D.D., Mittlefehldt, D.W., Wang, M.S., Keller, L., Lipschutz, M.E., Lindstrom, M.M., Garrison, D., 1994. Comparison of the LEW88516 and ALHA77005 Martian meteorites: similar but distinct. Meteoritics 29, 581–592.
Usui, T., Alexander, C.M.O., Wang, J., Simon, J.I., Jones, J.H., 2012. Origin of water and mantle–crust interactions on Mars inferred from hydrogen isotopes and volatile element abundances of olivine-hosted melt inclusions of primitive shergottites. Earth Planet. Sci. Lett. 357–358, 119–129.
Usui, T., McSween, H.Y., Floss, C., 2008. Petrogenesis of olivine-phyric shergottite Yamato 980459, revisited. Geochim. Cosmochim. Acta 72, 1711–1730.
Wadhwa, M., Crozaz, G., 1995. Trace and minor elements in minerals of nakhlites and Chassigny: clues to their petrogenesis. Geochim. Cosmochim. Acta 59, 3629–3645.
Wadhwa, M., 2001. Redox state of Mars' upper mantle and crust from Eu anomalies in shergottite pyroxenes. Science 291, 1527–1531.
Warren, P.H., Greenwood, J.P., Rubin, A.E., 2004. Los Angeles: a tale of two stones. Meteorit. Planet. Sci. 39, 137–156.
Xirouchakis, D., Draper, D.S., Schwandt, C.S., Lanzirotti, A., 2002. Crystallization conditions of Los Angeles, a basaltic Martian meteorite. Geochim. Cosmochim. Acta 66, 1867–1880.
Zhang, Y., Ren, Z.-Y., Xu, Y.-G., 2013. Sulfur in olivine-hosted melt inclusions from the Emeishan picrites: implications for S degassing and its impact on environment. J. Geophys. Res., Solid Earth 118, 4063–4070.
Zipfel, J., Schere, P., Spettel, B., Dreibus, G., Schultz, L., 2000. Petrology and chemistry of the new shergottite Dar al Gani 476. Meteorit. Planet. Sci. 35, 95–106.